AGU PUBLICATIONS

Geophysical Research Letters

RESEARCH LETTER
10.1002/2015GL064671

Key Points:
- Boundary scavenging is not enough to explain the Pa/Th ratios in Arctic
- Deep circulation mainly controls the Pa/Th distributions in Eurasian Basin
- Constrain on the deep circulation in Eurasian Basin during last glacial

Supporting Information:
- Figures S1–S4 and Table S1

Correspondence to:
Y. Luo,
ym537097@dal.ca

Citation:
Luo, Y. and J. Lippold (2015), Controls on ^{231}Pa and ^{230}Th in the Arctic Ocean, *Geophys. Res. Lett.*, *42*, 5942–5949, doi:10.1002/2015GL064671.

Received 23 MAY 2015
Accepted 2 JUL 2015
Accepted article online 3 JUL 2015
Published online 21 JUL 2015

Controls on ^{231}Pa and ^{230}Th in the Arctic Ocean

Yiming Luo[1] and Jörg Lippold[2]

[1]Department of Oceanography, Dalhousie University, Halifax, Nova Scotia, Canada, [2]Institute of Geological Sciences and Oeschger Centre for Climate Change Research, University of Bern, Bern, Switzerland

Abstract The distributions of ^{230}Th and ^{231}Pa in the Arctic Ocean are not well understood. In order to examine the Arctic ^{231}Pa/^{230}Th system and therefore to shed light on the future use of Arctic sedimentary ^{231}Pa/^{230}Th, we developed a 2-D scavenging model modified from an Atlantic model. Tuned with reasonable parameters that are consistent with Eurasian Basin geographic settings, the model can reproduce most of the features of the ^{230}Th and ^{231}Pa water column profiles as well as the sedimentary ^{231}Pa/^{230}Th distribution patterns and suggests that the sedimentary ^{231}Pa/^{230}Th in the Eurasian Basin is mainly controlled by the deep water circulation. In our attempt to reproduce the sedimentary ^{231}Pa/^{230}Th patterns during the last glacial, we found that circulation strength in the Eurasian Basin at shallower depths may have been stronger than today.

1. Introduction

In the Atlantic Ocean, sedimentary ^{231}Pa/^{230}Th (Pa/Th hereafter) ratios have been increasingly applied as a proxy for reconstructing past overturning circulation to study the glacial-interglacial variations of the Atlantic Meridional Overturning Circulation (AMOC) [*Böhm et al.*, 2015; *Bradtmiller et al.*, 2014; *Gherardi et al.*, 2009; *Lippold et al.*, 2012b; *McManus et al.*, 2004; *Yu et al.*, 1996]. This application is based on the shorter residence time of ^{230}Th (20–40 years) in sea water than ^{231}Pa (100–120 years) caused by the difference in their particle reactivity. Advection can thus redistribute ^{231}Pa more easily while ^{230}Th is mostly scavenged by settling particles to the local sediments. Therefore, smaller sedimentary Pa/Th ratios found in the Atlantic are interpreted as the result of high overturning rates. Vigorous lateral advection effectively removes ^{231}Pa from the deep Atlantic to the Southern Ocean, while low overturning rates result in higher sediment Pa/Th ratios when more ^{231}Pa is scavenged to the local Atlantic sediment [*Marchal et al.*, 2000].

A further observation supporting the use of sedimentary Pa/Th as indicator for circulation strength is the decrease of sedimentary Pa/Th with increasing water depth in the Atlantic Ocean basin. This behavior is a result of the persistent enhanced lateral transport of ^{231}Pa compared to ^{230}Th at all water depths. Reversible scavenging onto and from sinking particles leads to increasing concentrations of both ^{231}Pa and ^{230}Th with water depth [*Bacon and Anderson*, 1982], amplifying the relative ^{231}Pa depletion of deeper waters by advection. In the Atlantic Ocean with a current strong Northern Source Water overturning cell, this vertical effect in sedimentary Pa/Th is much more pronounced than the increase of Pa/Th with water mass age and lateral transport [*Luo et al.*, 2010]. Such a trend of decreasing Pa/Th with water depth was first observed in Southeast Atlantic sediments [*Scholten et al.*, 2008] and has been found also in a compilation of core tops at the Equatorial West Atlantic [*Lippold et al.*, 2011] and Atlantic sea water [*Deng et al.*, 2014]. It represents a general trend for Holocene Atlantic sediments [*Gherardi et al.*, 2009; *Lippold et al.*, 2012b]. However, it is important to note that strong circulation may produce high Pa/Th in shallower waters, as a result of enhanced scavenging of ^{231}Pa close to the surface combined with the downstream ingrowth of ^{231}Pa [*Luo et al.*, 2010].

Studies on water column distributions of ^{230}Th and ^{231}Pa or sedimentary Pa/Th in the Arctic [*Edmonds et al.*, 2004; *Edmonds et al.*, 1998; *Hoffmann and McManus*, 2007; *Moran et al.*, 2005; *Scholten et al.*, 1995] have been carried out in last 20 years, but there is still a lack of systematic understanding of the ^{230}Th and ^{231}Pa distributions. A recent study on the Arctic sedimentary Pa/Th by *Hoffmann et al.* [2013] revealed a pronounced deficit of ^{231}Pa in Arctic sediments for the past 35,000 years. Interestingly, the Arctic measurement results by *Hoffmann et al.* [2013] closely mirror the depth-dependent decrease of Pa/Th found in Atlantic sediments (Figure 1). While AMOC flux between 15 and 30 Sverdrup (Sv) can explain the observed Holocene ^{231}Pa/^{230}Th depth gradient, the same observation for the comparably sluggish Arctic

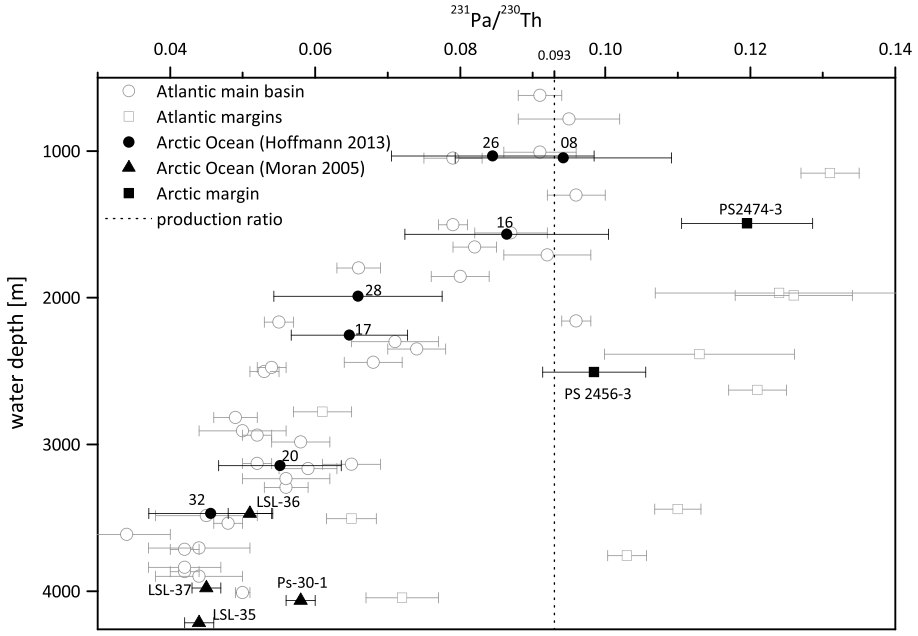

Figure 1. Holocene average Pa/Th [*Hoffmann et al*., 2013] (filled circle; numbers indicate location in Figure 2) and core tops [*Moran et al*., 2005] (filled triangle; Nansen and Amundsen Basin cores, green stars in Figure 2) from the Arctic Ocean show a very similar correlation to water depth as Pa/Th from the Atlantic main basin (circle) [*Lippold et al*., 2012b] (Holocene averages). Higher values (Holocene Pa/Th averages), with a more subtle depth gradient, are observed at margin cores or from high-latitude locations in the Atlantic (square) [*Lippold et al*., 2012b; *Roberts et al*., 2014]. Margin core tops from the Arctic (filled square; this study) show higher Pa/Th as well.

overturning (<7 Sv) [*Woodgate et al*., 2001] represents a conundrum for the interpretation of existing sedimentary Pa/Th data. An alternative potential sink for the missing Arctic ^{231}Pa could be boundary scavenging, wherein ^{231}Pa is exported from the lower-particle-flux central basin toward the higher-particle-flux margins [*Moran et al*., 2005].

In this study, we try to systematically explain the influence of Arctic deep water circulation on the ^{230}Th and ^{231}Pa distributions in the Arctic. We measured ^{231}Pa/^{230}Th from Arctic margin sediments in order to test the boundary scavenging hypothesis. Further, by adapting an Atlantic 2-D scavenging model [*Luo et al*., 2010] to the Arctic conditions, we aimed to reproduce representative Arctic water column ^{231}Pa and ^{230}Th profiles as well as Holocene sedimentary ratios using a circulation scheme consistent with the state-of-art configurations of the Arctic deep water circulation. We also attempted to constrain the Arctic circulation during the last glacial based on available sedimentary Pa/Th data.

2. Methods

2.1. Study Area

The deep water in the Arctic deep basin is mainly characterized by inflow of Atlantic water and outflow of Arctic deep water, both through the Fram Strait between Greenland and the Svalbard Archipelago (Figure 2).

Deep water formation in the Arctic Ocean is mainly the result of brine release due to freezing [*Rudels*, 2012]. This is countered by the inflow from the Nordic seas into the Atlantic, estimated to be about 7 Sv in total [*Rudels*, 2012] primarily at intermediate depth, with 6 ± 1 Sv as boundary current approaching the Lomonosov Ridge before it splits into two branches [*Woodgate et al*., 2001]. One branch with 3 ± 1 Sv turns back toward Fram Strait along the Lomonosov Ridge and another with 3 ± 1 Sv flows to the west of the ridge in the cyclonic boundary current. The volume of the Eurasian Basin is estimated at about $5.36 \cdot 10^6$ km^3 (Figure S1 in the supporting information) based on data from ETOPO1 Global Relief Model [*Eakins and Sharmann*, 2012], with an according residence time of the Eurasian Basin deep water of about 60 years if we take 3 Sv as the average ventilation strength.

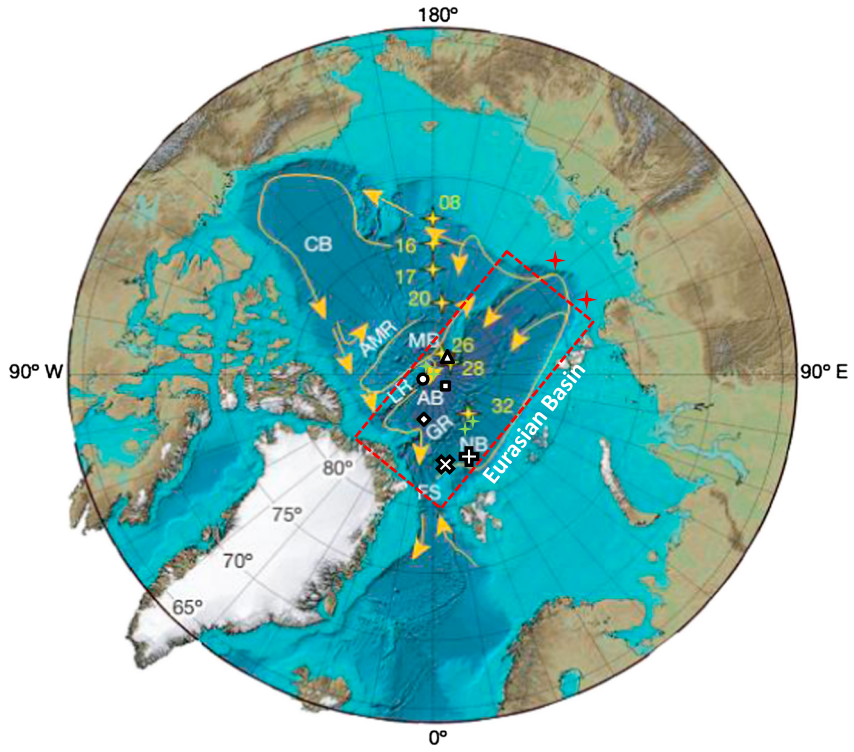

Figure 2. Map of the study area; reworked from Figure 1 in *Hoffmann et al.* [2013]. Acronyms in the figure are as follows: CB, Canada basin; AMR, Alpha-Mendeleev Ridge; MB, Makarov Basin; LR, Lomonosov Ridge; AB, Amundsen Basin; GR, Gakkel Ridge; NB, Nansen Basin; FS, Fram Strait. Locations of sediment cores are indicated by yellow stars and numbers as indicated in Figure 1 [*Hoffmann et al.*, 2013], green stars [*Moran et al.*, 2005], or red stars (this study). Water column profiles of ^{231}Pa and ^{230}Th in the Arctic Ocean [*Edmonds and Moran*, 2004; *Scholten et al.*, 1995] are represented by marks identical to the symbols in Figure 3. Arrows indicate patterns of intermediate and deep circulation.

This rough estimation shows that exchange rates in the deep Arctic Basin are basically not very different from those in the Atlantic Ocean. The relative narrowness of the Arctic Basin leads to residence times of water masses even slightly shorter than that of Atlantic waters. This provides the basis to apply a 2-D scavenging model as used by *Luo et al.* [2010] in the Atlantic to study the distributions of ^{230}Th and ^{231}Pa in the Arctic. We focus our study on the Eurasian Basin because more measurements on water column ^{230}Th, ^{231}Pa [*Edmonds and Moran*, 2004; *Scholten et al.*, 1995], and sedimentary Pa/Th [*Hoffmann et al.*, 2013] in this region were carried out, compared to those in the Amerasian Basin.

2.2. Model Parameterization

The two-dimensional model is based on a simple reversible scavenging model for both ^{230}Th and ^{231}Pa and a prescribed 2-D overturning scheme (please refer to *Luo et al.* [2010] for details regarding the model). The Eurasian Basin is treated as a 2-D overturning field with depth of 4000 m and length of 20° latitudinal distance, spanning virtually from Fram Strait (80°, 0°) to the head of Lomonosov Ridge (80°, 140°). The 2-D section is divided into 128 boxes with 16 grids on depth (250 m each) and 8 grids on latitude (2.5° each). Northward inflow of 2 Sv, as a conservative estimation of the circulation strength in the Eurasian Basin, from Fram Strait (80°, 0°) governs 0–750 m and extends to the head of Lomonosov Ridge. This water gradually deepens in the last four columns between (90°, 0°) and (80°, 140°). Southward flowing Arctic deep water dominates the depths below 750 m (supporting information Figure S1). The only change in parameter settings of the model compared to *Luo et al.* [2010] is that adsorption rate of ^{231}Pa is adjusted by a factor of 0.75 (compared to the Atlantic; supporting information Table S1), to take into account the small export productivity (EP) in the Arctic [*Cai et al.*, 2010]. Note that a steady state fractionation factor of 10.5 is derived from the above settings, which is consistent with the fractionation factor found in low-productivity regions [*Moran et al.*, 2002; *Walter et al.*, 1997]. In a next step, a plain flow scheme was adopted (supporting information Figure S2), which produces reasonable agreements to the observed ^{230}Th and ^{231}Pa water

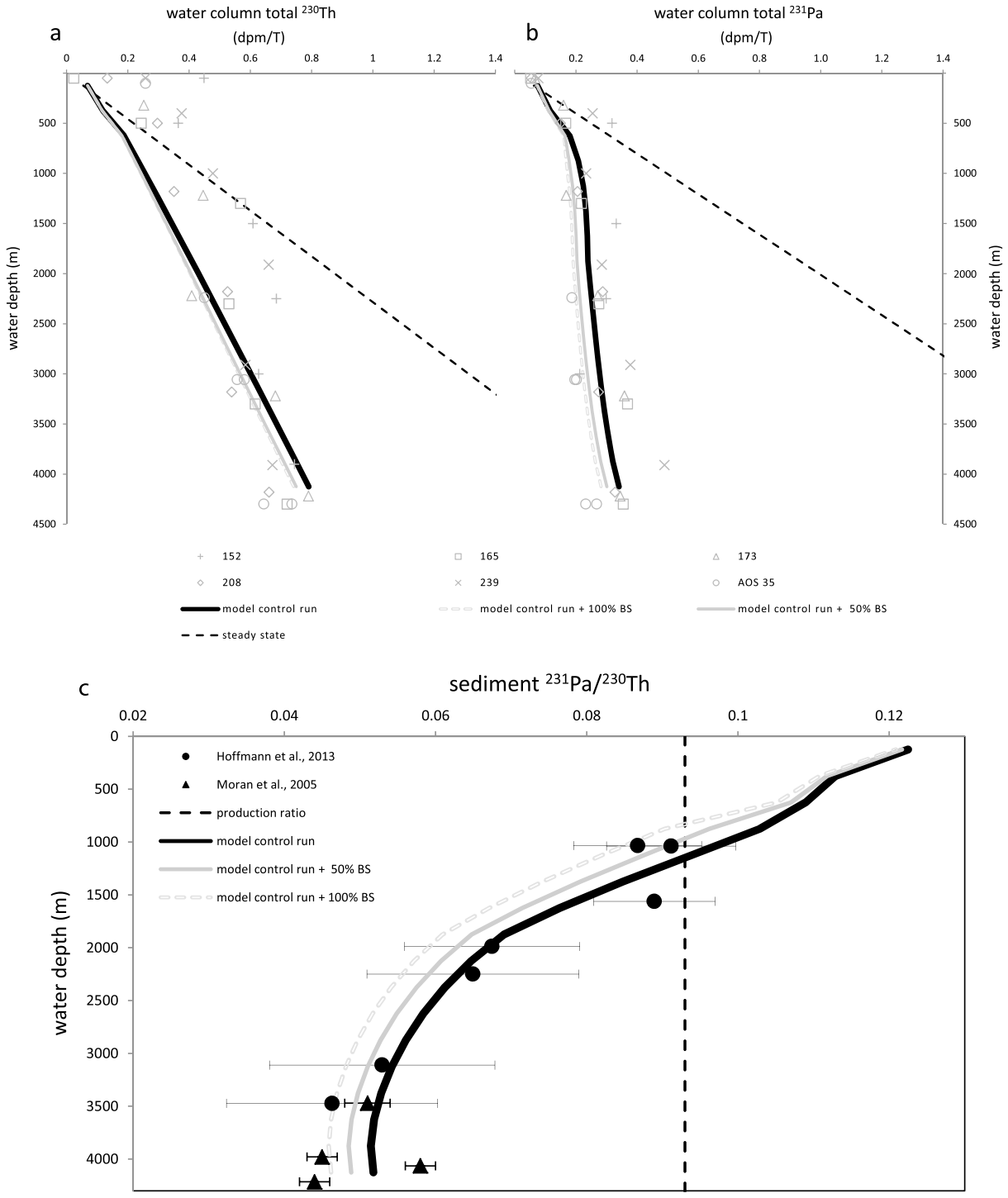

Figure 3. Water column (a) ^{230}Th and (b) ^{231}Pa profiles [*Edmonds and Moran*, 2004; *Scholten et al*., 1995] and (c) Holocene [*Hoffmann et al*., 2013] and core top [*Moran et al*., 2005] sedimentary Pa/Th ratios (2 standard deviation (SD) error bars) compared to model outputs. Shown are the control run with optimal model conditions and 2 Sv overturning strength (black) and modified control runs with two boundary scavenging intensities (grey).

column profiles (Figure 3). Further, a horizontal removal term is introduced into the model to take into account the influence of boundary scavenging on the distribution of ^{230}Th and ^{231}Pa in the open ocean. The strength of this removal term is, however, difficult to determine for the Eurasian Basin. We thus use a better defined boundary scavenging strength in the North Pacific as reference [*Luo*, 2013; *Roy-Barman*, 2009], which was a

Table 1. Measurement Results (Bulk Concentrations), Resulting Excess Pa/Th, and Geographic Parameters From PS 2456-3 [*Fütterer*, 1994] and PS 2474-3 [*Schoster*, 2005]

Core	Latitude North	Longitude East	Water Depth (m)	Sample Depth	Pa/Th	^{231}Pa (dpm/g)[a]	^{230}Th (dpm/g)	^{232}Th (dpm/g)	^{238}U (dpm/g)
PS 2456-3	78.48	133.03	2507	0–5 cm	0.098 (Error 2 SD = 0.007)	0.27 (Error 2 SD = 1.64%)	3.34 (Error 2 SD = 1.91%)	2.02 (Error 2 SD = 0.73%)	1.78 (Error 2 SD = 1.20%)
PS 2474-3	77.67	118.58	1494	0–5 cm	0.120 (Error 2 SD = 0.009)	0.30 (Error 2 SD = 1.75%)	3.20 (Error 2 SD = 2.10%)	1.82 (Error 2 SD = 0.76%)	2.02 (Error 2 SD = 1.24%)

[a]Disintegrations per minute (dpm).

depth-dependent removal term estimation based on the ^{230}Th and ^{231}Pa profiles measured in station "Aloha" and station "Papa" in the North Pacific. We applied the removal term with two different efficiencies (100% and 50%) in order to assess the importance of boundary scavenging compared to ventilation strength.

2.3. Measurements of Sedimentary Pa/Th

In order to examine the effect of boundary scavenging in the Arctic Ocean Pa/Th from two core top sediment samples from the margin of the Laptev Sea, which is particle rich due to being a sea ice factory and thus an ideal place to test for boundary scavenging, have been measured (Table 1). The chemical and analytical process was identical to the methods described by *Böhm et al*. [2015]. Measurements were performed on a Thermo Finnigan Element 2 at the University of Heidelberg (Germany). The contributions of lithogenic and authigenic ^{231}Pa and ^{230}Th were corrected by assuming a lithogenic background ^{238}U/^{232}Th [*Henderson and Anderson*, 2003] of 0.6 for this region [*Hoffmann et al*., 2013].

3. Results and Discussion

3.1. Sedimentary Pa/Th From the Slopes

Our new core top Pa/Th measurements from the Laptev Sea feature values of 0.098 and 0.120, respectively. Boundary scavenging indeed produces increased Pa/Th values compared to the Pa/Th values at comparable water depths as reported by *Hoffmann et al*. [2013]. However, the relatively moderate shift toward higher values cannot account for the observed total basin deficit in ^{231}Pa. This is the case simply because the smaller and shallower margins would need to show by far higher ratios in order to balance the missing ^{231}Pa from the much larger volume of the Eurasian Basin [*Jakobsson*, 2002] (see supporting information for ^{231}Pa budget estimation). This situation is very similar to the margins of the Atlantic Ocean (Figure 1), where boundary scavenging also leads to higher values than compared to the same water depth in the open ocean but cannot account for the huge deficit of the whole basin [*Lippold et al*., 2012a].

3.2. Water Column ^{230}Th and ^{231}Pa Distributions in the Eurasian Basin

Latitudinal or longitudinal trends of the ^{230}Th and ^{231}Pa distributions (total) in the Eurasian Basin are difficult to see (Figures 3a and 3b), due to the sparse data coverage and possible fast mixing of the water within the basin. Therefore, we compare observations with the latitudinal average of total ^{230}Th and total ^{231}Pa output in the entire 2-D sections excluding the last two model columns, where water deepening takes place (supporting information Figure S2). Note that this is the same approach used for our sedimentary Pa/Th model-data comparison in section 3.3.

Thorium-230 and Protactinium-231 concentrations in the study area are lower than comparable data in other low-productivity ocean regions such as the subtropical Pacific [*Roy-Barman*, 2009]. Such low concentrations contradict a weak vertical scavenging intensity due to low EP [*Cai et al*., 2010] in this region. We therefore attribute this observation mainly to ^{230}Th and ^{231}Pa removal by ventilation and export of deep waters from this region. Compared to the steady state linear profiles of ^{230}Th and ^{231}Pa, huge deficits in observed and modeled water column concentrations can be identified (dashed lines, Figures 3a and 3b). The ^{230}Th deficits at depth are identical to that found in the deep north Atlantic, while ^{231}Pa deficits are even more pronounced because of the weak vertical scavenging of ^{231}Pa. Model runs with weaker (50%) and full (100%) boundary scavenging efficiency did not result in significantly different ^{231}Pa and ^{230}Th distributions (Figure 3). This finding further suggests that boundary scavenging is most likely not the main reason for the missing Arctic ^{231}Pa.

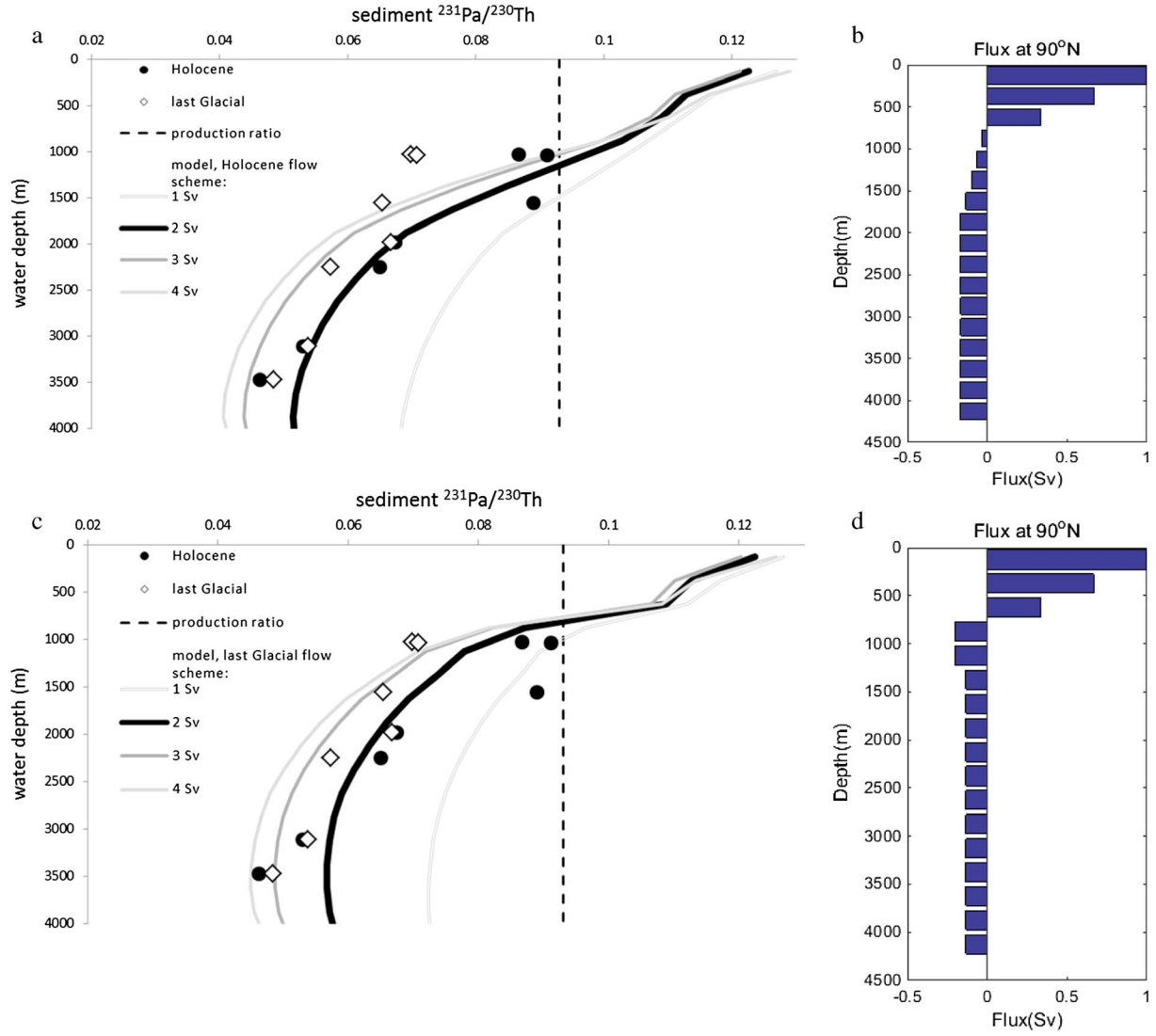

Figure 4. (a) Sedimentary Pa/Th in the Eurasian Basin in Holocene (filled circle) and last glacial (diamond) Arctic sediments [*Hoffmann et al.*, 2013] compared to the model outputs with the (b) deep circulation scheme and (c) compared to a (d) shallower (glacial) circulation scheme. The 2-D flow pattern for 2 Sv are shown in Figures 4b and 4d with positive fluxes at 90°N standing for northward flux, and negative fluxes standing for southward. For model runs with lower (1 Sv) or higher (3 or 4 Sv) total overturning strengths the proportional flux for each depth was kept constant.

3.3. Sedimentary Pa/Th in the Eurasian Basin

Sedimentary Pa/Th in the Arctic shows a vertical trend decreasing with depth, also reproduced by the 2-D model (Figure 3c). In the Atlantic, North Atlantic Deep Water (NADW) spreading effectively transports ^{231}Pa to the south at depth, which results in increasing ^{231}Pa deficits with water depth (lower Pa/Th). In the Eurasian Basin, the situation is similar. Although the Arctic deep water flow rate is smaller than NADW flux, the ventilation effect on ^{231}Pa/^{230}Th in the Eurasian Basin is still strong simply because the volume of the Eurasian Basin is very small compared to the Atlantic basin. Therefore, the decreasing trend of sedimentary Pa/Th with depth in the Eurasian Basin is very likely caused by the deep water circulation in the basin, considering that our 2-D model comprehensively reproduced the water column ^{230}Th, ^{231}Pa, and sedimentary Pa/Th in the basin with reasonable parameterization (Figure 3).

We note that Sites 08, 16, 17, and 20 [*Hoffmann et al.*, 2013] are located in the Amerasian Basin rather than Eurasian Basin. They are still included in this comparison because they are all on the route of the boundary current that enters the Amerasian Basin directly from the Eurasian Basin (Figure 2). These sites therefore may have similar water properties as sites in the central Eurasian Basin.

3.4. Sedimentary Pa/Th in the Eurasian Basin During the Last Glacial

Having shown that deep water circulation may have a primary control on the Holocene Pa/Th in the Eurasian Basin, we attempt to deduce the deep water circulation in the Eurasian Basin during the last glacial from the differences in the sedimentary Pa/Th during the two periods. The Pa/Th distribution pattern below 2000 m during the last glacial is generally consistent with the Pa/Th distribution in Holocene sediments (Figure 4a). But at water depths above 2000 m, the sedimentary Pa/Th during last glacial is clearly lower than Holocene Pa/Th.

We first tried to adjust the circulation rate with the same circulation scheme (Figure 4b) in order to reproduce the profile, but even doubling the total flow rate cannot satisfyingly reproduce the signal. This is primarily because flow rates between 800 and 2000 m are not strong enough to generate adequate ^{231}Pa deficits at these depths under the modern circulation pattern, and thus, increase in intermediate depth circulation strength during the Last Glacial Maximum as argued by *Cronin et al.* [2012] may be necessary. We thus adapted the circulation flow scheme in the 2-D field by promoting the flow rates at intermediate depth while reducing the flow rates in the deep ocean (Figures 4c and 4d). In this way, the sedimentary Pa/Th patterns during last glacial can be better reproduced with slightly stronger circulation, or with the same circulation strength but with joint effects of increased boundary scavenging and weakened vertical particle scavenging (Figure S4). However, promoted circulation strength at intermediate depth is the key to approach the low sediment Pa/Th ratio at these depths (Figure S4). This suggests that circulation in Eurasian Basin during last glacial was strong and more of its strength must have been shallower compared to today's conditions. Our results therefore do not support an isolated Arctic Basin during the last glacial, and the Arctic Ocean may not account for extremely radiocarbon-poor waters observed south of Iceland during cold intervals [*Thornalley et al.*, 2011]. A possible explanation for such values would have been the flushing out of ^{14}C-depleted deep waters from the Arctic Ocean, if the Arctic were isolated for a few thousand years.

4. Conclusion

New measurements from the Arctic Ocean margin revealed higher Pa/Th values compared to the main Eurasian Basin, but not enough to account for the generally low Pa/Th in this basin. From this finding, we have approached the observed ^{231}Pa versus ^{230}Th deficit in the Arctic Eurasian Basin from a circulation point of view. With a 2-D scavenging model adapted from the Atlantic model [*Luo et al.*, 2010] with Arctic parameterization, water column ^{230}Th and ^{231}Pa profiles in the Eurasian Basin as well as the vertical sedimentary Pa/Th patterns in the Arctic Ocean can be reasonably reproduced. Our findings imply deep circulation in the Arctic to have a primary control on the ^{230}Th and ^{231}Pa distributions in the basin, which raises the possibility to use the sedimentary Pa/Th in the Arctic to constrain the past changes of deep circulation in the Arctic.

We also made a first attempt to constrain the deep circulation in Eurasian Basin during the last glacial using available data. Our attempt points at a circulation regime that may have been stronger than today with increased vigor at shallower depth compared to today, in concert with conclusions based on Mg/Ca proxies [*Cronin et al.*, 2012]. We note this is a rough constraint only, given the limited information on the sedimentary Pa/Th in this region.

In order to better understand the evolution of the Arctic deep circulation during last glacial-interglacial transition, insights into the mechanism that controls the sedimentary Pa/Th ratios in Amerasian Basin and Canada Basin are important as well. Future work may focus on model work on the Pa/Th system in those basins. Improved data coverage of the sedimentary Pa/Th in the Arctic regions is urgently required.

Acknowledgments

Y. Luo wants to thank Bernard P. Boudreau for his financial support from his NSERC Discovery Fund. J. Lippold was supported by the FP7-PEOPLE-2013-IEF, Marie Curie proposal 622483. We thank Benny Antz and Stefan Rheinberger for analytical support. Our data (Table 1) are available to the public, and codes of the model will be provided upon request to Y. Luo.

The Editor thanks two anonymous reviewers for their assistance in evaluating this paper.

References

Bacon, M., and R. Anderson (1982), Distribution of thorium isotopes between dissolved and particulate forms in the deep sea, *J. Geophys. Res.*, *87*, 2045–2056, doi:10.1029/JC087iC03p02045.

Böhm, E., J. Lippold, M. Gutjahr, M. Frank, P. Blaser, B. Antz, J. Fohlmeister, N. Frank, M. B. Andersen, and M. Deininger (2015), Strong and deep Atlantic Meridional Overturning Circulation during the last glacial cycle, *Nature*, doi:10.1038/nature14059.

Bradtmiller, L. I., McManus, J. F., Robinson, L. F. (2014), 231Pa/230Th evidence for a weakened but persistent Atlantic meridional overturning circulation during Heinrich Stadial 1, *Nat. Commun.*, *5*, 5817, doi:10.1038/ncomms6817.

Cai, P., M. Rutgers van der Loeff, I. Stimac, E. M. Nothig, K. Lepore, and S. B. Moran (2010), Low export flux of particulate organic carbon in the central Arctic Ocean as revealed by 234Th:238U disequilibrium, *J. Geophys. Res.*, *115*, C10037, doi:10.1029/2009JC095595.

Cronin, T. M., G. S. Dwyer, J. Farmer, H. A. Bauch, R. F. Spielhagen, M. Jakobsson, J. Nilsson, W. M. Briggs Jr., and A. Stepanova (2012), Deep Arctic Ocean warming during the last glacial cycle, *Nat. Geosci.*, *5*, 631–634.

Deng, F., A. Thomas, M. Rijkenberg, and G. Henderson (2014), Controls on seawater 231Pa, 230Th and 232Th concentrations along the flow paths of deep waters in the Southwest Atlantic, *Earth Planet. Sci. Lett.*, *390*, 93–102.

Eakins, B. W., and G. F. Sharmann (2012), *Hypsographic Curve of Earth's Surface From ETOPO1*, NOAA Natl. Geophys. Data Center, Boulder, Colo.

Edmonds, H., S. Bradley Moran, J. A. Hoff, J. N. Smith, and R. L. Edwards (1998), Protactinium-231 and Thorium-230 Abundances and High Scavenging Rates in the Western Arctic Ocean, *Science*, *280*, 405–407.

Edmonds, H. N., S. B. Moran, H. Cheng, and R. L. Edwards (2004), 230Th and 231Pa in the Arctic Ocean: Implications for particle fluxes and basin-scale Th/Pa fractionation, *Earth Planet. Sci. Lett.*, *227*, 155–167.

Fütterer, D. K. (1994), The Expedition ARCTIC '93 Leg ARK-IW4 of RV "Polarstern" 1993, Reports on Polar Research, AWI Bremerhaven, pp. 1–244.

Gherardi, J., L. Labeyrie, S. Nave, R. Francois, J. McManus, and E. Cortijo (2009), Glacial-interglacial circulation changes inferred from $^{231}Pa/^{230}Th$ sedimentary record in the North Atlantic region, *Paleoceanography*, *24*, PA2204, doi:10.1029/2008PA001696.

Henderson, G., and R. Anderson (2003), The U-series toolbox for paleoceanography, Uranium Series Geochemistry, *Rev. Mineral. Geochem.*, *128*, 493–531.

Hoffmann, S., and J. McManus (2007), Is there a 230Th deficit in Arctic sediments, *Earth Planet. Sci. Lett.*, *258*, 516–527.

Hoffmann, S., J. McManus, W. Curry, and L. S. Brown-Leger (2013), Persistent export of ^{231}Pa from the deep central Arctic Ocean over the past 35,000 years, *Nature*, *497*, 603–607.

Jakobsson, M. (2002), Hypsometry and volume of the Arctic Ocean and its constituent seas, *Geochem. Geophys. Geosyst.*, *3*, 1–18, doi:10.1029/2001GC000302.

Lippold, J., J. Gherardi, and Y. Luo (2011), Testing the $^{231}Pa/^{230}Th$ paleocirculation proxy—A data versus 2D model comparison, *Geophys. Res. Lett.*, *38*, L20603, doi:10.1029/2011GL049282.

Lippold, J., S. Mulitza, G. Mollenhauer, S. Weyer, and M. Christl (2012a), Boundary scavenging at the east Atlantic margin does not negate use of Pa/Th to trace Atlantic overturning, *Earth Planet. Sci. Lett.*, *333–334*, 317–331.

Lippold, J., Y. Luo, R. Francois, S. Allen, J. Gherardi, S. Pichat, B. Hickey, and H. Schulz (2012b), Strength and geometry of the glacial Atlantic Meridional Overturning Circulation, *Nat. Geosci.*, *5*, 813–816.

Luo, Y. (2013), The influence of deep water circulation on the distribution of ^{231}Pa and ^{230}Th in the water column and sediments of the Pacific Ocean, PhD thesis, chap. 4, Univ. of British Columbia, Vancouver.

Luo, Y., R. Francois, and S. Allen (2010), Sediment $^{231}Pa/^{230}Th$ as a recorder of the rate of the Atlantic meridional overturning circulation: Insights from a 2-D model, *Ocean Sci.*, *6*, doi:10.5194/os-5196-5381-2010.

Marchal, O., R. Francois, T. Stocker, and F. Joos (2000), Ocean thermohaline circulation and sedimentary $^{231}Pa/^{230}Th$ ratio, *Paleoceanography*, *15*, 625–641, doi:10.1029/2000PA000496.

McManus, J., R. Francois, J. Gherardi, L. Keigwin, and S. Brown-Leger (2004), Collapse and rapid resumption of Atlantic meridional circulation linked to deglacial climate change, *Nature*, *428*, 834–837.

Moran, S., C. Shen, R. Edwards, H. Edmonds, J. Scholten, J. Smith, and T.-L. Ku (2005), ^{231}Pa and ^{230}Th in surface sediments of the Arctic Ocean: Implications for $^{231}Pa/^{230}Th$ fractionation, boundary scavenging, and advective export, *Earth Planet. Sci. Lett.*, *234*, 235–248.

Moran, S. B., C. C. Shen, H. N. Edmonds, S. E. Weinstein, J. N. Smith, and R. L. Edwards (2002), Dissolved and particulate Pa-231 and Th-230 in the Atlantic Ocean: Constraints on intermediate/deep water age, boundary scavenging, and Pa-231/Th-230 fractionation, *Earth Planet. Sci. Lett.*, *203*, 999–1014.

Roberts, N., J. McManus, A. Piotrowski, and N. McCave (2014), Advection and scavenging controls of Pa/Th in the northern NE Atlantic, *Paleoceanography*, *29*, 668–679, doi:10.1002/2014PA002633.

Roy-Barman, M. (2009), Modelling the effect of boundary scavenging on thorium and protactinium profiles in the ocean, *Biogeosciences*, *6*, 3091–3107.

Rudels, B. (2012), Arctic Ocean circulation and variability–advection and external forcing encounter constraints and local processes, *Ocean Sci.*, *8*, 261–286.

Scholten, J., J. Fietzke, A. Mangini, D. Garbe-Schönberg, A. Eisenhauer, P. Stoffers, and R. Schneider (2008), Advection and Scavenging: Effect on ^{230}Th and ^{231}Pa distribution off Southwest-Africa, *Earth Planet. Sci. Lett.*, *271*, 159–169.

Scholten, J. C., M. M. Rutgers van der Loeff, and A. Michel (1995), Distribution of 230Th and 231Pa in the water column in relation to the ventilation of the deep Arctic basins, *Deep Sea Res. Part II*, *42*, 1519–1531.

Schoster, F. (2005), Terrigenous sediment supply and paleoenvironment in the Arctic Ocean during the late Quaternary: Reconstructions from major and trace elements, in *Reports on Polar and Marine Res.*, R.o.P.M. (Ed.), p. 149.

Thornalley, D. J. R., S. Barker, W. S. Broecker, H. Elderfield, and I. N. McCave (2011), The deglacial evolution of North Atlantic deep convection, *Science*, *331*, 202–205.

Walter, H.-J., M. M. R. Van der Loeff, and H. Hoeltzen (1997), Enhanced scavenging of ^{231}Pa relative to ^{230}Th in the South Atlantic south of the Polar Front: Implications for the use of the $^{231}Pa/^{230}Th$ ratio as a paleoproductivity proxy, *Earth Planet. Sci. Lett.*, *149*, 85–100.

Woodgate, R. A., K. Aagaard, R. D. Muench, J. Gunn, G. Björk, B. Rudels, A. T. Roach, and U. Schauer (2001), The Arctic Ocean Boundary Current along the Eurasian slope and the adjacent Lomonosov Ridge: Water mass properties, transports and transformations from moored instruments, *Deep Sea Res., Part I*, *48*, 1757–1792.

Yu, E., R. Francois, and M. Bacon (1996), Similar rates of modern and last-glacial ocean thermohaline circulation inferred from radiochemical data, *Nature*, *379*, 689–694.